Available online at www.sciencedirect.com
SCIENCE DIRECT
Journal of the European Ceramic Society 26 (2006) 1259–1266
www.elsevier.com/locate/jeurceramsoc

# Electrically conductive SiC–$(Nb,Ti)_{ss}$–$(Nb,Ti)C_{ss}$ cermet

M. Balog [a,*], P. Šajgalík [a], F. Hofer [b], P. Warbichler [b], K. Fröhlich [c], O. Vávra [c], J. Janega [d], J.-L. Huang [e]

[a] *Institute of Inorganic Chemistry, Slovak Academy of Sciences, Bratislava, Slovakia*
[b] *Research Institute for Electron Microscopy and Fine Structure, University of Technology, Graz, Austria*
[c] *Institute of Electrical Engineering, Slovak Academy of Sciences, Bratislava, Slovakia*
[d] *Faculty of Materials Science and Technology, Slovak Technical University, Trnava, Slovakia*
[e] *Department of Materials Science and Engineering, National Cheng Kung University, Tainan, Taiwan, ROC*

Received 16 June 2004; received in revised form 21 December 2004; accepted 10 January 2005
Available online 22 March 2005

**Abstract**

The present paper deals with the processing method of SiC–$(Nb,Ti)_{(ss)}$–$(Ti,Nb)C_{(ss)}$ composites. The electrically conductive phases were formed by in situ reaction: $NbC_{(s)} + Ti_{(s)} \rightarrow (Nb,Ti)_{(ss)} + (Ti,Nb)C_{(ss)}$ that takes place during the reaction sintering by hot pressing. Prepared composites exhibit good compromise between electrical and mechanical properties and the present approach allows preparing a wide variety of compositions. For example composites containing 80 wt.% SiC and 20 wt.% $\{(Nb,Ti)_{(ss)}$–$(Ti,Nb)C_{(ss)}\}$ have an electrical resistivity $2.6 \times 10^{-4}\ \Omega\,m$, hardness 21.6 GPa and fracture toughness 6.3 MPa $m^{1/2}$.


*Keywords:* SiC; Cermets; Electrical properties; Interface; Electron microscopy

## 1. Introduction

SiC based ceramics is one of the most studied synthetic materials of the last century. This interest is based on the extraordinary properties of SiC, which predominantly are high hardness, oxidation resistance, and shock resistance as well as good strength.[1–6] Recently, the liquid phase sintering of SiC was developed.[7–9] Metal oxide with the $SiO_2$ as a main impurity of SiC powder create the liquid at the sintering temperature of SiC and enhance densification process similarly to those known for $Si_3N_4$ ceramics. By using $Al_2O_3$ or $Al_2O_3/Y_2O_3$ as sintering additive the SiC ceramics was densified almost to the full density at the temperatures below 2000 °C.[7–9]

SiC based ceramics is a hard material with the Vickers hardness varying from 22 to 26 GPa.[1] This fact substantially increases the difficulty with the machining of the structural part made of SiC. The diamond machining tools are usually used for the final shaping which makes the cost of the particular SiC structural part very expensive. Other possibility of machining of hard materials is a discharge machining but this technique requires the electrically conductive structural material. This is not the case for SiC, which has an electrical resistivity of ∼0.1 Ω m at room temperature.[1]

The review of the literature data showed that the papers on the SiC with a metal-like electrical conductivity are relatively rare in the literature.[10,11] On the other hand, a relatively large fraction of the papers deal with the improvement of mechanical properties of ceramics by addition of the metal particles.[12–14]

By combination of both approaches the new SiC based composite/cermet could be developed. Such composite would have a metal-like electrical conductivity with a mechanical properties as good as liquid phase sintered SiC. The present paper deals with the processing of such SiC based cermets, where the Nb-based metallic alloy is designed as the metallic constituent securing the metallic conductivity as

* Corresponding author.
*E-mail address:* uachbalo@savba.sk (M. Balog).

0955-2219/$ – see front matter © 2005 Elsevier Ltd. All rights reserved.
doi:10.1016/j.jeurceramsoc.2005.01.038

well as ductile bridging of the crack. Mechanical properties as hardness and fracture toughness simultaneously with the electrical resistivity of all compositions are reported.

## 2. Experimental

Starting mixtures with the chemical compositions listed in Table 1 were ball milled in isopropyl alcohol with SiC balls for 24 h. The used powders were as follows: β-SiC powder (Superior Graphite, USA), $Y_2O_3$ (H.C. Starck, Germany), $Yb_2O_3$ (H.C. Starck, Germany), $Sm_2O_3$ (Stigma, Russia), AlN (H.C. Starck, Germany), Ti (TOHO Titanium Co., Japan) and NbC (Japan New Metals Co., Japan).

The compositions of the starting mixture was based on the following rules: weight ratio of SiC:AlN:$M_2O_3$ was kept constant, 87:3:10, where $M_2O_3$ is a metal oxide. The molar ratio of particular oxides was kept constant 1:1 for all compositions. The addition of Ti and NbC was increasing as it is listed in Table 1; the weight ratio of both constituents was kept 1:1.8.

The only exception is the sample N, Table 1, which contains no SiC as well as oxide additives, but the ratio of Ti:NbC was the same as written above. All powder mixtures were ball milled in isopropyl alcohol with SiC balls for 24 h. The homogenized suspension was dried, subsequently sieved through 25 μm sieve screen in order to avoid large hard agglomerates. Axially pressed samples of 12 mm in diameter and 10 mm high were embedded in BN and located into graphite die. All samples were hot pressed in two steps: firstly at 1650 °C for 3 h allowing to proceed the reaction producing the desired electrically conductive phases (Nb,Ti) and (Nb,Ti)C and secondly at 1850 °C for 1 h under mechanical pressure of 30 MPa in Ar atmosphere allowing to densify the ceramic–metal composite. The same two-step heat treatment was carried out with the sample N. Densities of cooled samples were measured by Archimedes method in mercury. The theoretical densities were calculated according to the rule of mixtures. The hot-pressed materials were cut, polished, and plasma etched with $CF_4$ +10% $O_2$ gas mixture for the microstructure analysis. The microstructures were observed by scanning electron microscopy (SEM, Zeiss EVO 40) and transmission electron microscopy. Analytical transmission electron microscopy was performed using a Gatan imaging filter mounted on a Philips CM20 TEM/STEM (acceleration voltage 200 kV, equipped with $LaB_6$ cathode). By dimpling of SiC composite of thickness 100 μm a thickness of about 20 μm was achieved: the thin foil was then ion-milled until perforation.[15,16] Chemical analyses were done by electron dispersive X-ray analysis (EDX) and electron energy loss spectroscopy (EELS), respectively.

Vickers hardness and fracture toughness were measured using LECO Hardness tester (Model LV-100AT, LECO, USA) by indentation method with a loads of 9.8 N and 98 N, respectively. Fracture toughness was calculated using the formula of Shetty.[17] Electrical resistivity was performed by four probes method at 25 °C. Ultrasonically soldered indium pads were used as contacts.

## 3. Thermodynamic background

Electrically conductive alloys were designed according to the following reaction:

$$NbC_{(s)}+Ti_{(s)} \rightarrow (Nb,Ti)_{(ss)}+(Ti,Nb)C_{(ss)} \quad (1)$$

The phase equilibrium diagram of Nb–Ti–C system at temperature 1700 °C in Fig. 1, McHale[18] shows that products of the reaction (1) lay on the line connecting Ti and NbC. Their composition and state (solid or liquid) are depending on the chemical composition of the starting mixture. Formation of the liquid phase should be avoided, because liquid metal could be squeezed out from the ceramic matrix when hot pressing is used as the consolidation method. No liquid is formed in A + D region of the phase diagram. Point N shown by the arrow represents the composition chosen for this study. The composition N lies in the solid-state region up to 2000 °C when first liquid appears.

Table 1
Chemical composition of samples

| Samples | Composition in wt.% | | | | | | |
|---|---|---|---|---|---|---|---|
| | SiC | AlN | $Y_2O_3$ | $Yb_2O_3$ | $Sm_2O_3$ | Ti | NbC |
| SC–Y | 87 | 3 | 10 | – | – | – | – |
| SC–10N–Y | 78.3 | 2.7 | 9 | – | – | 3.60 | 6.40 |
| SC–20N–Y | 69.6 | 2.4 | 8 | – | – | 7.14 | 12.86 |
| SC–50N–Y | 43.5 | 1.5 | 5 | – | – | 17.85 | 32.15 |
| SC–80N–Y | 17.4 | 0.6 | 2 | – | – | 28.55 | 51.45 |
| SC–90N–Y | 8.7 | 0.3 | 1 | – | – | 32.12 | 57.88 |
| SC–YbSm | 87 | 3 | – | 5.30 | 4.70 | – | – |
| SC–20N–Yb/Sm | 69.6 | 2.4 | – | 4.24 | 3.76 | 7.14 | 12.86 |
| SC–50N–Yb/Sm | 43.5 | 1.5 | – | 2.65 | 2.35 | 17.85 | 32.15 |
| N | – | – | – | – | – | 35.6 | 64.4 |

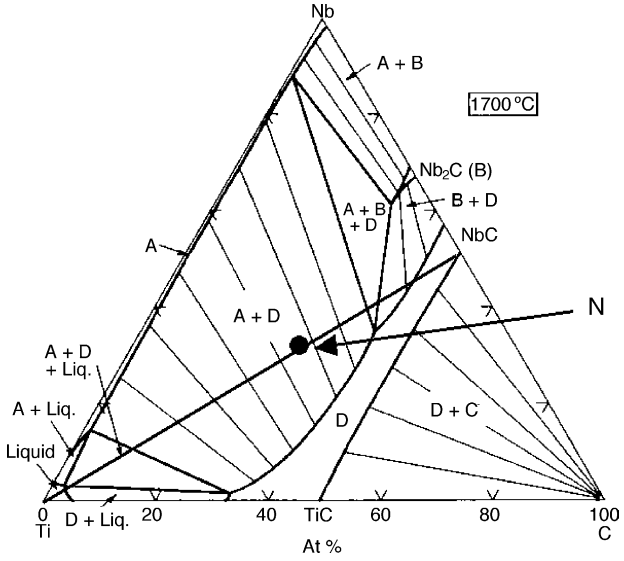


Fig. 1. Phase equilibrium diagram of Ti–Nb–C system at 1700 °C,[15] where A = $(Nb,Ti)_{(ss)}$, B = $Nb_2C$, C = TiC and D = $(Ti,Nb)C_{(ss)}$; N is the desired composition of the electrically conductive phase.

The melting point of Ti is 1668 °C and thus reaction (1) must be conducted below this temperature in order to avoid the formation of metal liquid. That is the reason why the temperature of 1650 °C was suggested for the reaction step. Temperature of 1850 °C was chosen for the subsequent densification step of the SiC–$(Nb,Ti)_{ss}$–$(Nb,Ti)C_{ss}$ system by hot pressing. The two-step sintering process, reaction step at 1650 °C and densification step at 1850 °C, should lead to the desired final composition of the metal–ceramic composite.

## 4. Results

### *4.1. Microstructure of SiC ceramics and SiC–$(Nb,Ti)_{ss}$–$(Nb,Ti)C_{ss}$ composite*

The microstructures of hot pressed samples SC–Y, SC–10N–Y, SC–50N–Y and SC–80N–Y are shown in Fig. 2. The microstructure of SC–Y consists of plate-like SiC grains, with the size up to 10 μm and thickness up to 2 μm, Fig. 2a. The 10 wt.% addition of composition N has a small influence on the SiC grain size and shape, Fig. 2b. With increasing addition of composition N, up to 50 wt.% the grain size of SiC grains is getting smaller (approximately 2 μm) and also the shape of the grains is changed to the more equiaxed, Fig. 2c. The distribution of SiC islands in the 80 wt.% of composition N is documented in Fig. 2d.

EDX analysis of sample SC–YbSm, Fig. 3, shows, that the phase at the triple junction of SiC grains consists mostly of $Yb_2O_3$, $Sm_2O_3$ and $SiO_2$. The same can be concluded for the other samples where the composition of the triple points also reflects the kind of the oxide additions to the starting composition.

The typical microstructure of the SC–20N–Y composite, similar to those shown in Fig. 2, is shown in Fig. 4. The composition N is overetched, while the SiC grains are good visible. The N particles are randomly distributed within the SiC matrix. No continual network of particles of composition N is observed for the SiC matrix containing 20 wt.% of N. The evolution of the SiC microstructure along with the increasing content of composition N is shown in Figs. 2b–d. Plasma etching did not allow to visually distinguish whether composition N consists of one or more phases, Figs. 2 and 4.

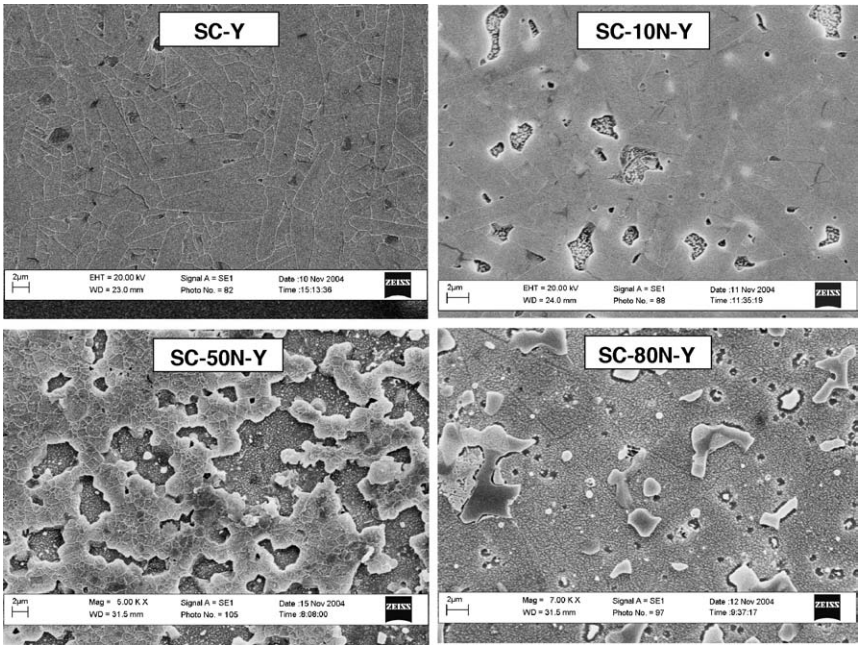


Fig. 2. Microstructure of the (a) SC–Y, (b) SC–10N–Y, (c) SC–50N–Y and (d) SC–80N–Y samples.

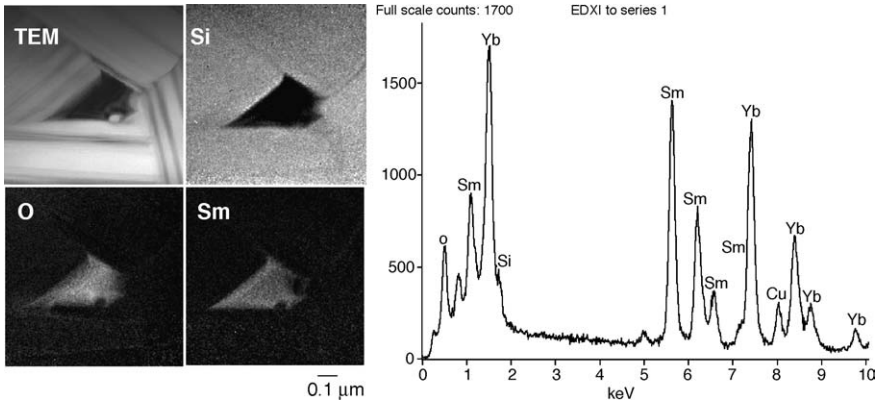


Fig. 3. TEM bright field image of sample SC–YbSm, EFTEM elemental maps (Si, O, Sm) and the EDX spectrum of the triple point.

### 4.2. Microstructure of metallic phases

The TEM bright field image of electrically conductive composition N is shown in Fig. 5. The sample was prepared by the two-step sintering process described in Section 2. The reason to apply this processing was to check the final composition of the electrically conductive N-phase after the same processing as for SC–*x*N–Y/Yb,Sm ($x = 0$, 10, 20, 50, 80, 90 wt.%) composites. As it results from EELS analysis in Fig. 5, composition N consists of two different phases:

- solid solution of $(Nb,Ti)_{ss}$ metallic phases, and
- solid solution of ceramic $(Nb,Ti)C_{ss}$ phases.

EDX analysis of the cermet sample SC–50N–YbSm shows that composite consists of at least four phases (Fig. 6). The major phase is SiC (EDX1), the other phases are a solid solution of $(Nb,Ti)_{ss}$ and $(Nb,Ti)C_{ss}$ (EDX2), a phase consisting of $SiO_2$–$Yb_2O_3$–$Sm_2O_3$ (EDX3) and additionally a (Si,Nb,Ti)O phase was identified (EDX4).

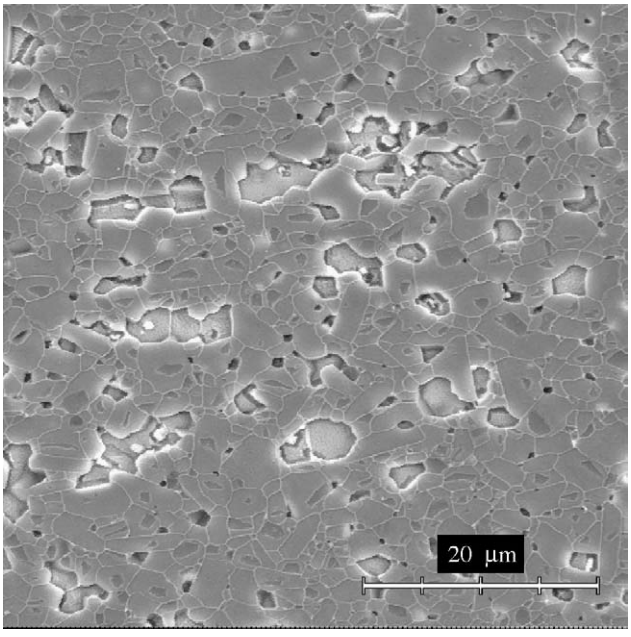


Fig. 4. SEM micrograph of the composition SC–20N–Y. Grains of composition N are overetched.

### 4.3. Mechanical properties

The micro-hardness and indentation fracture toughness of selected compositions are shown in Figs. 7 and 8, respectively. As it is visible from the both graphs, the mechanical properties are not substantially changed by the addition of the $(Nb,Ti)_{ss}$ and $(Nb,Ti)C_{ss}$ phases up to 50 wt.% of their addition.

### 4.4. Electrical resistivity

Fig. 9 shows the dependence of the electrical conductivity of the SC–*x*N–Y/Yb,Sm ($x = 0$, 10, 20, 50, 80, 90 wt.%) composites on the addition of the $(Nb,Ti)_{ss}$ and $(Nb,Ti)C_{ss}$ phases. The almost linear decrease of the resistivity up to 80 wt.% of addition of the electrically conductive N-phases is observed. Above this value the resistivity of the composite is not remarkably changed.

## 5. Discussion

As Fig. 2 shows the mean grain size of SiC microstructure decreased by the increased addition of the $(Nb,Ti)_{ss}$ and $(Nb,Ti)C_{ss}$ phases in the SC–*x*N–Y ($x = 0$, 10, 50, 80 wt.%) composites. This is probably a result of presence of $(Nb,Ti)_{ss}$ and $(Nb,Ti)C_{ss}$ phases, which hinder the grain boundary migration as well as are responsible for the prolongation of the diffusion paths leading to the SiC grain growth. The $(Nb,Ti)_{ss}$ and $(Nb,Ti)C_{ss}$ phases SC–*x*N–Y/Yb,Sm ($x = 0$, 10, 20, 50, 80, 90 wt.%) composites principally consist of four phases: SiC, $(Nb,Ti)_{ss}$, $(Nb,Ti)C_{ss}$ and (Si,Nb,Ti)O glass phase. All these phases have a crucial importance on the composite behavior. The results of Figs. 7 and 8 show that $(Nb,Ti)_{ss}$, $(Nb,Ti)C_{ss}$ phases have negligible influence on the hardness and fracture toughness of the SiC–[$(Nb,Ti)_{ss}$, $(Nb,Ti)C_{ss}$] composite up to 50 wt.% of their addition. According to

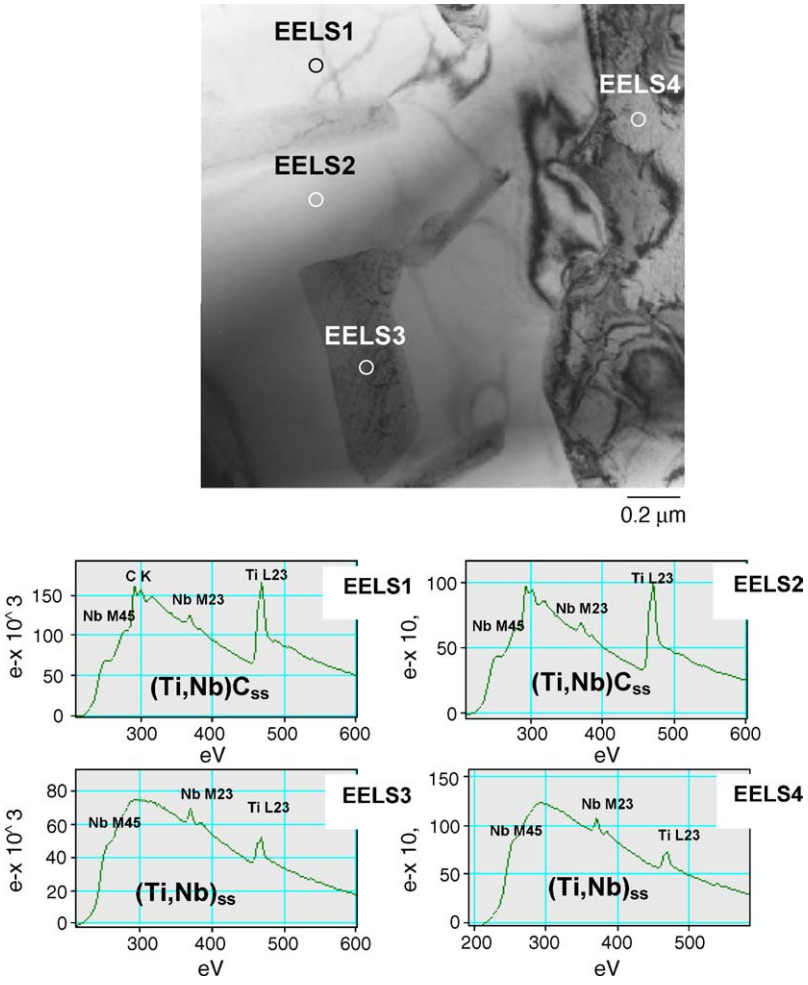


Fig. 5. Bright field TEM image of the composition N and the corresponding EELS analyses.

the phase diagram, Fig. 1, point N consists of ~30 at.% of $(Nb,Ti)_{ss}$ and 70 at.% of $(Nb,Ti)C_{ss}$, respectively. Probably low amount and low plasticity of metallic $(Nb,Ti)_{ss}$ phase caused its negligible influence on the fracture toughness. On the other hand, almost not changed hardness, Fig. 7 is probably a result of partial positive contribution of ceramic $(Nb,Ti)C_{ss}$ phase.

Fig. 8 shows that the electrical resitivity of SiC–[$(Nb,Ti)_{ss}$, $(Nb,Ti)C_{ss}$] composite decreases almost proportionally with the addition of both $(Nb,Ti)_{ss}$ and $(Nb,Ti)C_{ss}$ phases. Interestingly, the decrease (1–3 orders of magnitude) is observed already at small additions of $(Nb,Ti)_{ss}$, $(Nb,Ti)C_{ss}$ phases, 10 and 20 wt.%, respectively, Fig. 9. This was not expected because the typical percolation behavior was anticipated for this composite. The percolation threshold was expected at approximately 20 vol.% of addition of the $(Nb,Ti)_{ss}$ and $(Nb,Ti)C_{ss}$ phases when a continuous network of electrically conductive phases is formed. This threshold was found out for other systems by Lenčéš et al.[19] In the case of Fig. 9, theoretically 20 wt.% of $(Nb,Ti)_{ss}$ and $(Nb,Ti)C_{ss}$ phases formed in situ corresponds to the approximately 12 vol.%, i.e. the system has not enough electrically conductive phases for such remarkable decrease of the resistivity. As implies from Fig. 4, no continuous network of these phases was observed in the SC–20N–Y composite. Thus, the decrease of the electrical resistivity must be related to other effect, most probably to the presence of other conductive phases in the SC–10/20N–Y composites. Fig. 6a shows the oxygen, titanium and niobium maps of the composite. The oxygen map indicates the presence of continuous oxide phase also on the grain boundaries between SiC and $(Nb,Ti)_{ss}$, $(Nb,Ti)C_{ss}$ phases. The EDX-analysis of area 4 in Fig. 6b confirms a presence of small amount of a (Si,Nb,Ti)O phase. This phase is probably an inherent part of grain boundary phase. It could be proposed that presence of Nb and Ti in the $SiO_2$ glass could lead to the electrical conductivity of this glass. When this (Si,Nb,Ti)O phase is distributed along the all grain boundaries, this fact could lead to the conclusion that this phase is responsible for the increased overall conductivity of the SC–10/20N–Y composite. Overall electrical conductivity of the composite is given by conductivity of the (Si,Nb,Ti)O grain boundary phase and $(Nb,Ti)_{ss}$, $(Nb,Ti)C_{ss}$ phases. While the first mentioned glass phase increase the electrical conductivity of the SC–10/20N–Y composite at the low amounts of $(Nb,Ti)_{ss}$,

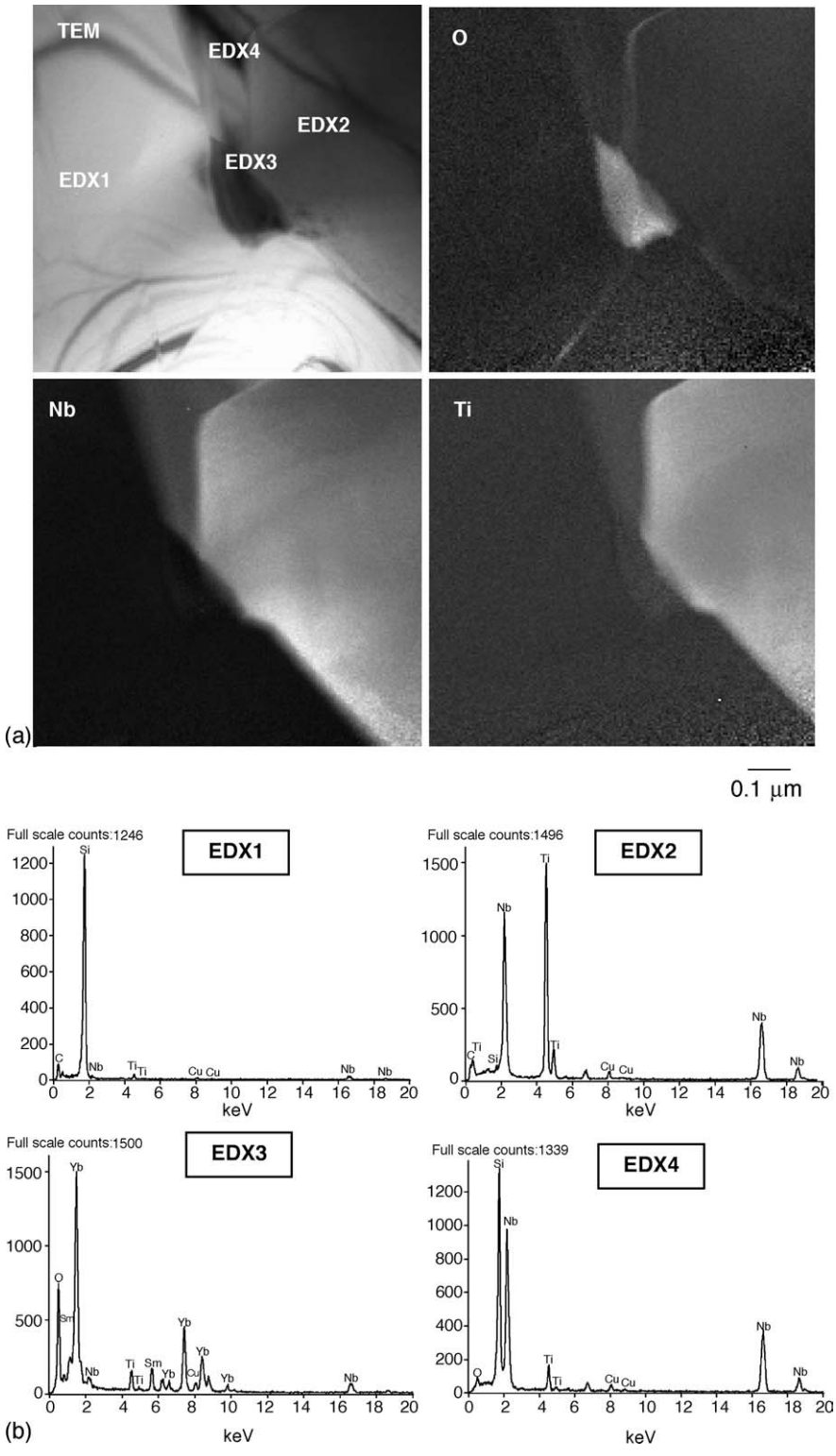


Fig. 6. (a) Bright field TEM and EFTEM elemental maps (O, Nb and Ti) of the composite SC–50N–Y. (b) EDX analyses of the positions shown in TEM.

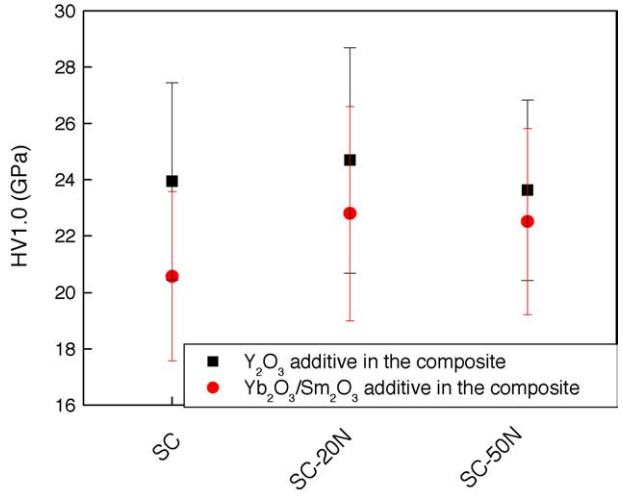


Fig. 7. Vickers hardness of the SiC–$(Nb,Ti)_{ss}$–$(Nb,Ti)C_{ss}$ composites measured at the load of 9.81 N, on samples containing different sintering agents.

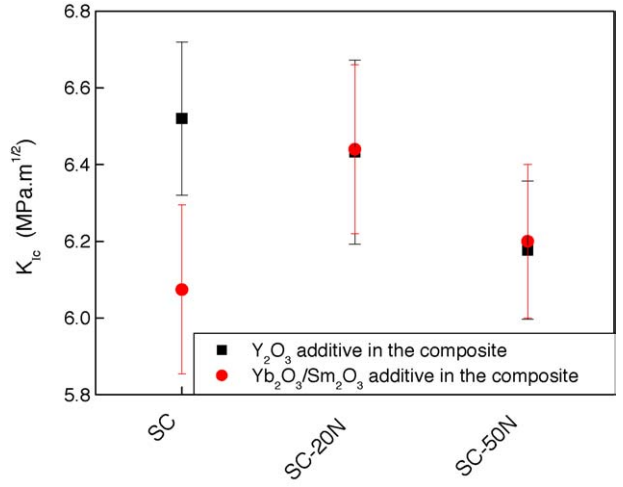


Fig. 8. Fracture toughness of the SiC–$(Nb,Ti)_{ss}$–$(Nb,Ti)C_{ss}$ composites measured at the load of 98.1 N by the indentation method, on samples containing different sintering agents.

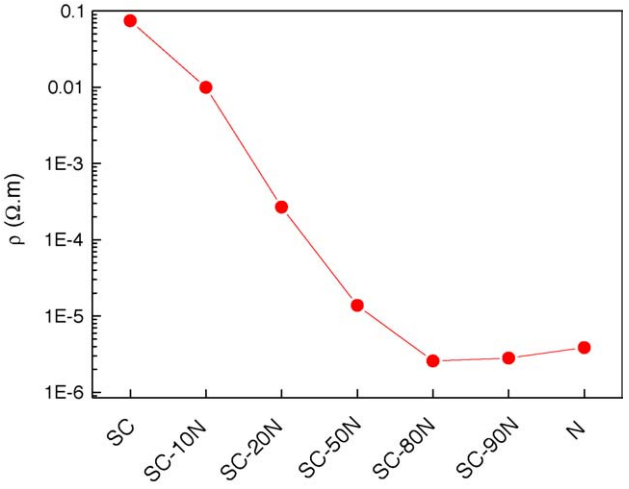


Fig. 9. Resistivity of the SC–*x*N–Y ($x = 0$, 10, 20, 50, 80, 90 wt.%) and N composite measured by four probes method.

$(Nb,Ti)C_{ss}$ phases, the last mentioned phases undertake the main role when they form the continuous network, i.e. at the addition >20 wt.%.

## 6. Conclusions

SiC based cermets were successfully prepared in the present work. The electrically conductive $(Nb,Ti)_{ss}$–$(Nb,Ti)C_{ss}$ phases were created in situ during densification of the starting composition. Composites were prepared in two-step processing. In the first step (reaction step), the electrically conductive phase $(Nb,Ti)_{ss}$–$(Nb,Ti)C_{ss}$ is formed. The second step (densification step) enabled the formation of a dense ceramic–metal composite. The occurrence of $(Nb,Ti)_{ss}$–$(Nb,Ti)C_{ss}$ phases were confirmed by EDX and EELS analysis. Hardness and fracture toughness were not substantially changed by the addition of the $(Nb,Ti)_{ss}$ and $(Nb,Ti)C_{ss}$ phases up to 50 wt.%. Their values are 23 GPa and 6 MPa $m^{1/2}$, respectively. An almost linear decrease of electrical resistivity up to 80 wt.% of the electrically conductive phases was observed. Above this value the electrical resistivity of the composite was not remarkably changed and kept the constant value of $\sim 10^{-6}\ \Omega$ m.

## Acknowledgements

Financial support of the Slovak Grant Agency, project No. VEGA 2/4072/24, VEGA 2/3101/23, grant 2003 ŠO 51/03R 06 00/03R 06 03, APVT-51-049702 and Centrum Excellence NANOSMART is gratefully acknowledged.

## References

1. Schneider, S. J., *Engineered Materials Handbook, Vol 4*. ASM International, USA, 1987, pp. 807–808.
2. Lee, S.-H., Lee, Y.-I., Kim, Y.-W., Xie, R.-J., Mitomo, M. and Zhang, G.-D., Mechanical properties of hot-forget silicon carbide ceramics. *Scripta Mater.*, 2005, **52**, 153–156.
3. Miyazaki, H., Hakomori, A., Yasuda, K., Matsuo, Y., Yano, T. and Iseki, T., Densification and thermal, mechanical and electrical properties of SiC ceramics sintered with addition of MgO. *J. Ceram. Soc. Jpn.*, 2001, **109**(3), 227–231.
4. Biswas, K., Rixecker, G. and Aldinger, F., Effect of rare-earth cation assition on the high temperature oxidation behaviour of LPS–SiC. *Mater. Sci. Eng. A*, 2004, **374**, 56–63.
5. Babayants, G. I. and Lanin, A. G., Thermal stress resistance and heat-induced damage of silicon carbide materials for laser mirrors. *J. Eur. Ceram. Soc.*, 2000, **20**, 1515–1520.
6. Hannink, R. H., Bando, Y., Tanaka, H. and Inomata, Y., Microstructural investigation and indentation response of pressureless-sintered α- and β-SiC. *J. Mater. Sci.*, 1988, **23**, 2093–2101.
7. Sciti, D. and Bellosi, A., Effects of additives on densification, microstructure and properties of liquid-phase sintered silicon carbide. *J. Mater. Sci.*, 2000, **35**, 3849–3855.
8. Choi, H.-J. and Lee, J.-G., Oxidation behavior of liquid-phase sintered silicon carbide with aluminium nitride and rare-earth oxides ($Re_2O_3$, where Re = Y, Er, Yb). *J. Am. Ceram. Soc.*, 2002, **85**(9), 2281–2286.

9. Zhou, Y., Hirao, K., Toriyama, M., Yamauchi, Y. and Kanzaki, S., Effects of intergranular phase chemistry on the microstructure and mechanical properties of silicon carbide ceramics densified with rare-earth oxide and alumina additions. *J. Am. Ceram. Soc.*, 2001, **84**(7), 1642–1644.
10. Duan, R.-G., Kuntz, J. D., Garay, J. E. and Mukherjee, A. K., Metal-like electrical conductivity in ceramic nano-composite. *Scripta Mater.*, 2004, **50**, 1309–1313.
11. Zhang, X., Lu, Z. and Jin, Z., Electrical resistivity and microstructure of pressureless reactive sintered $MoSi_2$–SiC composite. *Mater. Chem. Phys.*, 2004, **86**, 16–20.
12. Petit, F., Descamps, P., Poorteman, M., Cambier, F. and Leriche, A., Contribution of crack-bridging to the reinforcement of ceramics–metal composites/definition of an optimum particle size. *Key Eng. Mater.*, 2002, **206–213**, 1189–1192.
13. Peng, L. M., Cao, J. W. and Han, K. S., Mechanical properties of ceramic–metal composites by pressure infiltration of metal into porous ceramics. *Mater. Sci. Eng. A*, 2004, **374**, 1–9.
14. Raddatz, O., Schneider, G. A., Mackens, W., Voss, H. and Claussen, N., Bridging stresses and R-curves in ceramic/metal composites. *J. Eur. Ceram. Soc.*, 2000, **20**, 2261–2273.
15. Hofer, F. and Warbichler, P., Improved imaging of secondary phases in solids by energy-filtering TEM. *Ultramicroscopy*, 1996, **63**, 21–25.
16. Hofer, F., Warbichler, P. and Grogger, W., Nanoanalyse im Elektronenmikroskop. *Spectrum der Wissenschaft*, 1998, **10**, 48–54.
17. Shetty, D. K., Wring, I. G., Mincer, P. M. and Clauer, A. H., Indentation fracture of WC–Co cermets. *J. Mater. Sci.*, 1985, **20**, 1873–1882.
18. McHale, A. E., *Phase Equilibria Diagrams, Vol X*. The American Ceramics Society, 1994.
19. Lenčéš, Z., Šajgalík, P., Balog, M., Fröhlich, K. and Roncari, E., Layered $Si_3N_4$/(SiAlON + TiN) composites with self-diagnostic ability. *Ceramic Materials and Components for Engines*. Wiley-VCH, Weinheim, 2001, pp. 559–564.